

Frizzled7 Antibody-Functionalized Nanoshells Enable Multivalent Binding for Wnt Signaling Inhibition in Triple Negative Breast Cancer Cells

Rachel S. Riley and Emily S. Day*

Antibodies that antagonize cell signaling pathways specific to their targeted receptor are invaluable tools to study and treat malignancies, but their utility is limited by high production costs and treatment dosages. Researchers have shown that antibodies conjugated to nanoparticles display increased affinity for their target relative to freely delivered antibodies due to multivalency, and this study investigates how this multivalency can enable antibody–nanoparticle conjugates to inhibit oncogenic cell signaling more effectively than freely delivered antibodies. This effect was evaluated using triple negative breast cancer (TNBC) cells that are characterized by hyperactive Wnt signaling mediated through overexpressed Frizzled7 (FZD7) transmembrane receptors. Through analysis of the expression of β -catenin and Axin2, two downstream targets in the Wnt pathway, the results demonstrate that FZD7 antibody–nanoshell conjugates (FZD7-NS) are drastically more effective at inhibiting Wnt signaling in TNBC cells than freely delivered FZD7 antibodies. Additionally, cells treated with FZD7-NS, but not cells treated with freely delivered FZD7 antibodies, have decreased viability, indicating the therapeutic potential of this technology. The results demonstrate that antibody-functionalized nanoparticles can exploit multivalency for improved signal cascade interference over free antibodies, and this may ultimately permit lower antibody dosages to be administered to study signaling pathways or to manage diseases.

R. S. Riley, Dr. E. S. Day
Department of Biomedical Engineering
University of Delaware
161 Colburn Lab, 150 Academy Street
Newark, DE 19716, USA
E-mail: emilyday@udel.edu

Dr. E. S. Day
Department of Materials Science and Engineering
University of Delaware
Newark, DE 19716, USA

Dr. E. S. Day
Helen F. Graham Cancer Center and Research Institute
Newark, DE 19713, USA

 The ORCID identification number(s) for the author(s) of this article can be found under <https://doi.org/10.1002/sml.201700544>.

DOI: 10.1002/sml.201700544



1. Introduction

Antibodies have emerged as invaluable tools for the study and treatment of cancer because they can manipulate signaling pathways that drive cancer progression with high specificity.^[1,2] While antibodies can be designed to either agonize or antagonize specific receptors upon binding, they are most commonly used to obstruct prooncogenic signaling downstream of their targeted receptor by acting in an antagonistic manner.^[3] Although effective, antibodies are extremely expensive and require high dosages that can be cost-prohibitive or can produce adverse side effects, both of which limit their therapeutic success.^[4,5] To overcome these limitations, antibodies can be conjugated to nanoparticles (NPs) to enhance the target binding affinity due to multivalency, in

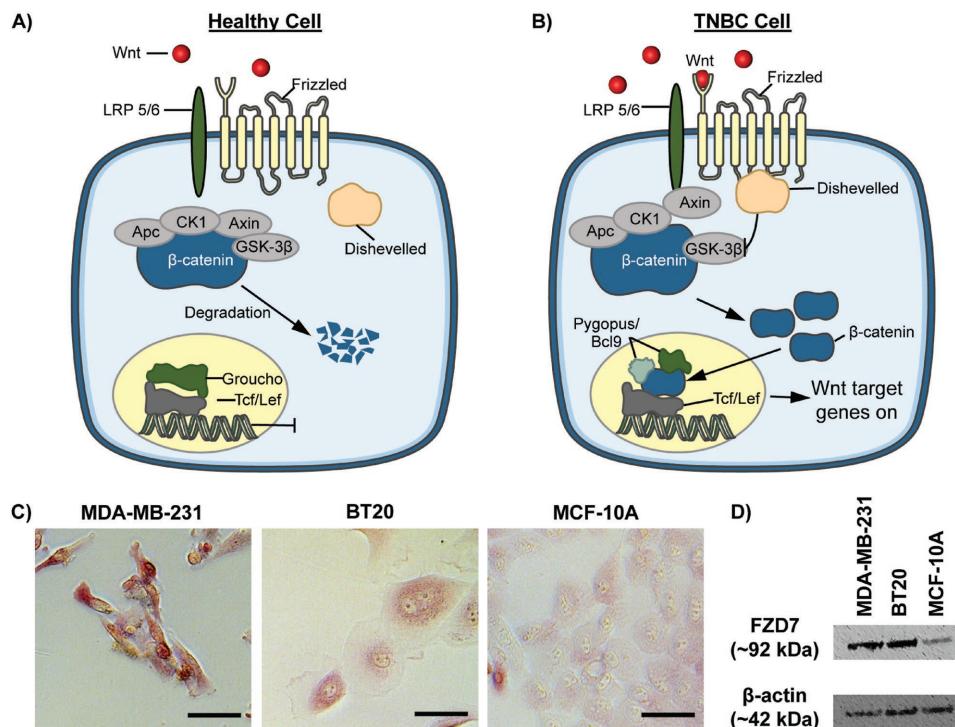


Figure 1. Schematic of the Wnt signaling pathway and validation of FZD7 overexpression in TNBC cells. A) In healthy cells, extracellular Wnt proteins are minimally available to bind Frizzled and LRP5/6 coreceptors. When Wnt signaling is inactive, a destruction complex composed of Apc, Axin, and GSK-3 β continuously regulates β -catenin expression by enabling its phosphorylation and subsequent degradation by GSK-3 β and CK1. B) In many cancers, including TNBC, extracellular Wnt proteins and Frizzled7 receptors are overexpressed, leading to hyperactive Wnt signaling. When Wnt proteins bind Frizzled and LRP5/6 coreceptors, Dishevelled is activated to inhibit the β -catenin destruction complex. Stabilized β -catenin accumulates in the cytoplasm and enters the nucleus to bind TCF/Lef transcription factors and activates Wnt target genes. C) Immunohistochemical staining and D) Western blotting of Frizzled7 expression (red in C) in MDA-MB-231 and BT20 TNBC cells versus noncancerous MCF-10A cells. Scale bars = 50 μ m.

which antibodies on NPs can engage multiple targeted antigens to increase the binding strength between ligand and receptor.^[6] In fact, multivalency is recognized as a means to improve upon targeted therapeutics that have defined biological properties.^[7] We hypothesized that multivalent binding could be exploited to specifically bind targeted cells and thus yield enhanced oncogenic cell signaling inhibition relative to free antibody delivery, and we tested this hypothesis using in vitro culture models of triple negative breast cancer (TNBC).

TNBC accounts for 15%–20% of diagnosed breast cancer cases and is associated with earlier relapse, higher mortality rates, and significantly decreased progression-free survival compared to other subtypes of breast cancer. The cells in TNBC tumors lack expression of the estrogen, progesterone, and human epidermal growth factor 2 receptors, rendering the disease unsusceptible to conventional targeted or hormonal therapies.^[8,9] Therefore, it is imperative to develop effective therapies specifically for this disease. A promising therapeutic target that has recently emerged as a driving force behind TNBC progression is the Wnt signaling pathway. Wnt signaling is a highly regulated process in healthy cells; normally, a destruction complex composed of adenomatous polyposis coli (APC), axin, glycogen synthase kinase-3 β (GSK-3 β), and casein kinase 1 (CK1) binds and phosphorylates β -catenin, leading to its constitutive degradation (**Figure 1A**).^[10–14] In contrast, Wnt signaling is activated in TNBC cells and other aggressive cancers when extracellular Wnt proteins, such as

Wnt3a, bind Frizzled (FZD), and LRP 5/6 receptors that are amplified on the cell surface, as shown in Figure 1B–D. This recruits Dishevelled to the cell membrane and blocks GSK-3 β activity to stabilize β -catenin and limit its degradation. Once stabilized, β -catenin accumulates in the cytoplasm and enters the nucleus where it associates with Tcf/Lef proteins to activate the transcription of Wnt target genes including Axin2, Cyclin D1, and c-Myc. Of these genes, Axin2 is the global downstream transcriptional target and main indicator of Wnt activity.^[15–17] While Wnt hyperactivity in some cancers is due to mutations in the genes encoding β -catenin or APC,^[18] in TNBC it is mainly due to increased expression of FZD7 receptors on the cell surface (this can be observed in Figure 1C,D, which show relative FZD7 expression in two TNBC cell lines and one noncancerous breast cell line). In fact, FZD7 is overexpressed in 67% of TNBC tumors and is the only member of the ten FZD family receptors that is significantly overexpressed.^[11,19,20] Accordingly, FZD7 provides an excellent biomarker for studying the effects of multivalent nanoparticle targeting on signaling cascade interference as described here.

Since Wnt ligands bind FZD7 receptors to initiate Wnt signaling in TNBC cells, we hypothesized that nanoshells (NS) coated with FZD7 antibodies (FZD7-NS) could competitively bind these receptors to block extracellular Wnt activation, leading to the destabilization of β -catenin and decreased Axin2 expression. Further, we expected that

FZD7-NS would have an amplified inhibitory effect on Wnt signaling relative to unconjugated FZD7 antibodies due to multivalency resulting in increased binding affinity towards FZD7 receptors. The potential of using FZD7 as a target for Wnt signaling inhibition and management of TNBC is supported by the fact that short hairpin RNA-mediated knock-down of FZD7 decreased β -catenin stabilization and nuclear localization in TNBC cells.^[20] Additionally, FZD7 antibodies have been proven effective against Wilms' tumor as a standalone therapy.^[21] Further, Gurney et al. demonstrated that OMP-18R5, an antibody against five of the ten FZD receptors, could inhibit Wnt signaling to decrease tumorigenicity and increase chemosensitivity in a variety of cancers.^[22] Interestingly, OMP-18R5 is currently being evaluated in clinical trials in combination with chemotherapy.^[23] However, a limiting factor of antibody therapies to treat cancer is that the high required treatment dosages may be cost prohibitive and lead to adverse side effects. Since inhibiting Wnt signaling has been shown to be effective for cancer treatment, and nanoparticle multivalency can enhance antibodies' target affinity, our goal in this work was to demonstrate that FZD7 antibodies conjugated to NS are more effective than freely delivered FZD7 antibodies. By capitalizing on multivalent binding effects to reduce the antibody dosage required for Wnt signaling inhibition, FZD7-NS could ultimately result in cheaper and safer treatment, making them an excellent platform for management of TNBC.

While our studies focus on using FZD7-NS to manipulate Wnt signaling in TNBC, from a broader perspective they provide important insight into the role of multivalency in signal cascade manipulation. The ability to enhance tumor cell specific binding or internalization of NPs with targeting agents like antibodies has been thoroughly investigated,^[24,25] but only recently have researchers begun to examine the impact of these targeted NPs on downstream signaling events.^[26,27] These studies are important because cell signaling manipulation by targeted nanoparticles is recognized as a promising therapeutic technique.^[28] The rationale for using antibody–nanoparticle conjugates rather than freely delivered antibodies is supported by the fact that improvements in therapeutic efficacy have been observed for other molecules conjugated to or encapsulated within NPs, including peptides,^[29] small interfering RNAs or microRNAs,^[30,31] chemotherapeutics,^[32–34] or a combination of these.^[26] The advantage of using antibodies to manipulate cellular signaling rather than small molecule inhibitors, gene regulation agents, or peptides, is that they offer high specificity and stability, and they do not require cellular uptake to be effective. The findings we report here contribute to an exciting new era of investigation regarding

the use of antibody-functionalized nanoparticles to block interactions between cancer cell receptors and their native ligands in the tumor microenvironment.

We used NS composed of 120 nm silica cores and 15 nm thick gold shells (**Figure 2**) as the base platform for this work because they enable simple gold–thiol bioconjugation chemistry to attach targeting ligands,^[24,25,35] have proven safety and biocompatibility in clinical trials,^[36] can be visualized with optical imaging modalities to track their cellular binding,^[37,38] and their size enables many antibodies to be conjugated to their surfaces. Additionally, because NS with this core diameter:shell thickness ratio maximally absorb near infrared light (≈ 800 nm), which penetrates tissue more deeply than other wavelengths of light, their in vivo distribution could be tracked with optical imaging modalities in future in vivo studies or they could be exploited for secondary treatment strategies such as photothermal therapy.^[35,39] We coated NS with FZD7 antibodies (FZD7-NS) and polyethylene glycol (PEG, for stabilization) and investigated their capabilities for Wnt signaling inhibition in an in vitro model of TNBC (**Figure 2**). Our data demonstrate that FZD7-NS can selectively bind cells overexpressing FZD7 to enable highly specific Wnt signaling inhibition (**Figure 3**). In the presence of the Wnt ligand Wnt3a, treating TNBC cells with FZD7-NS decreases β -catenin protein levels, ultimately leading to a $\approx 60\%$ decrease in Axin2 mRNA expression compared to cells treated with untargeted NS (**Figures 4 and 5**). This indicates that FZD7-NS competitively bind FZD7 receptors to

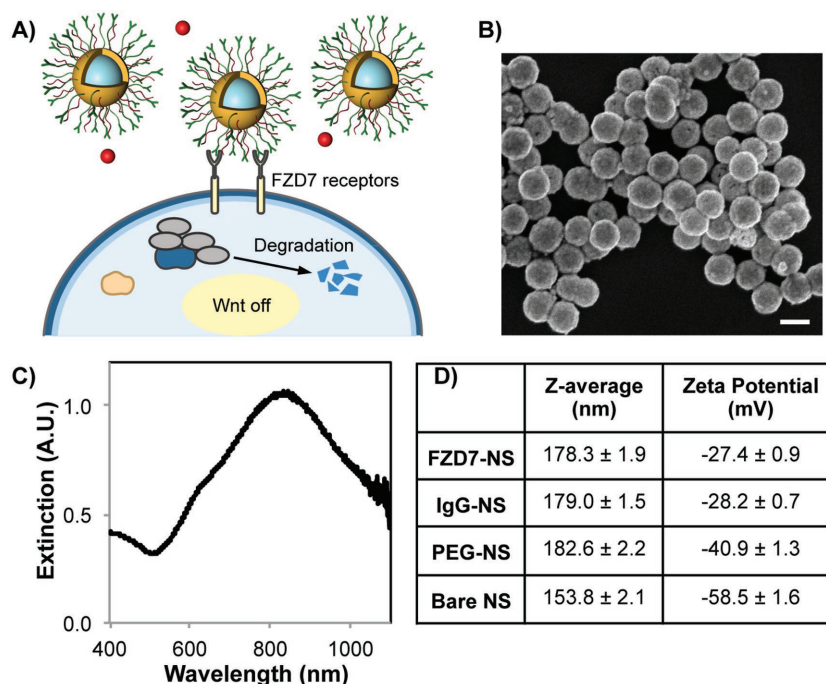


Figure 2. A) Silica core/gold shell nanoshells coated with Frizzled7 antibodies (green) and poly(ethylene) glycol (maroon) can bind FZD7 receptors multivalently to block extracellular Wnt activation by Wnt ligands (red), leading to the subsequent degradation of β -catenin. B) Scanning electron microscopy (SEM) image of bare nanoshells showing homogenous structure and complete gold shell. Scale bar = 150 nm. C) Plasmon resonant extinction spectra of nanoshells with peak absorbance at 830 nm. D) Dynamic light scattering (hydrodynamic diameter) and zeta potential measurements of nanoshell formulations.

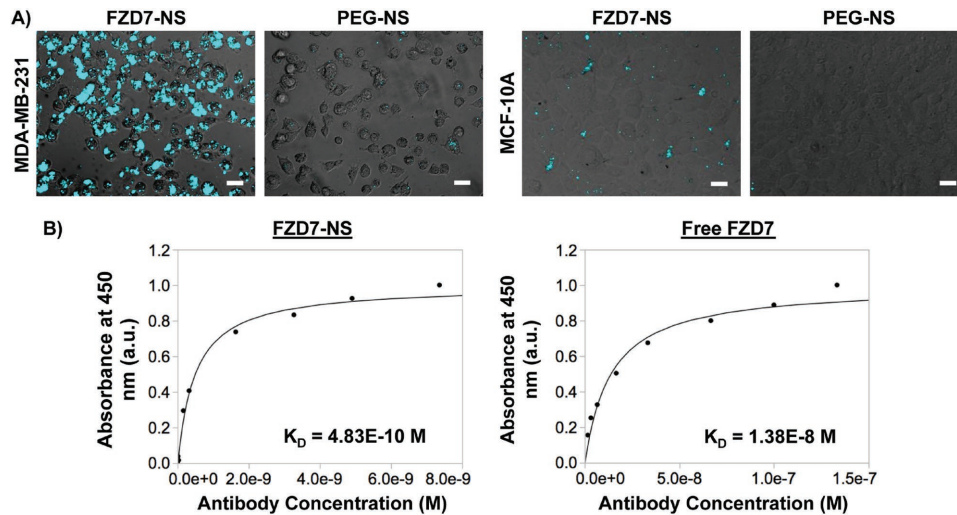


Figure 3. A) Two-photon microscopy showing binding capacity of FZD7-NS and PEG-NS (blue) to MDA-MB-231 and MCF10A cells, which express high and low levels of Frizzled7, respectively. Scale bars = 25 μ m. B) Effective dissociation constant of FZD7-NS (left) and free FZD7 antibodies (right) to MDA-MB-231 cells. Data was fit to a modified Langmuir isotherm model.

inhibit Wnt signaling. Interestingly, treating TNBC cells with ≈ 50 -fold excess of free FZD7 antibodies does not result in the same level of Wnt inhibition achieved with FZD7-NS, indicating that multivalent binding plays an important role in signal cascade manipulation. These results support the

continued development of antibody-functionalized nanoparticles for signal cascade interference in aggressive cancers that are driven by aberrant Wnt signaling, such as TNBC. Further, our results suggest that other researchers should carefully investigate the impact that targeted NPs have on

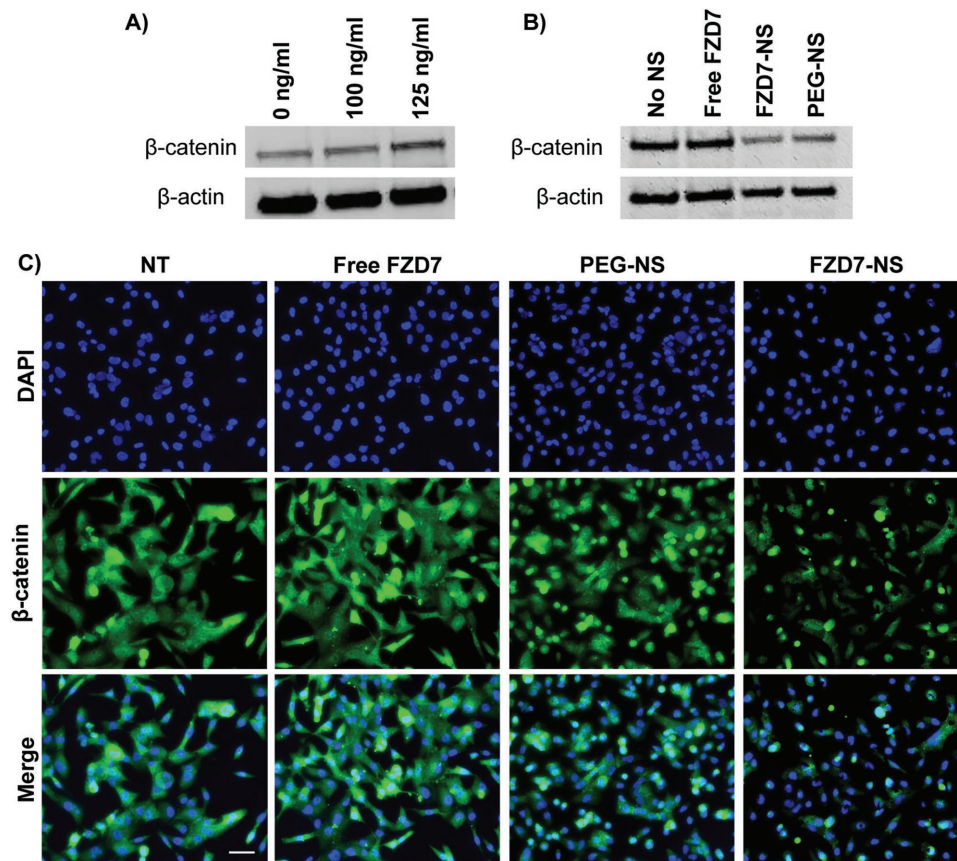


Figure 4. A) Western blotting showing β -catenin expression following treatment with 0, 100, or 125 ng mL⁻¹ Wnt3a for 4 h. B) Representative Western blot and C) immunofluorescence analysis showing β -catenin expression in MDA-MB-231 cells following treatment with free FZD7 antibodies, FZD7-NS, PEG-NS, or no NS in the presence of 125 ng mL⁻¹ Wnt3a. Scale bar = 50 μ m.

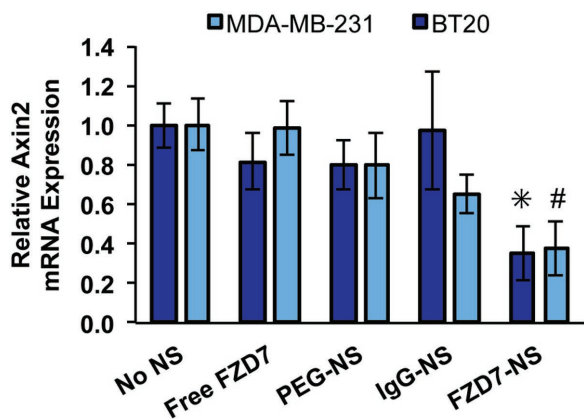


Figure 5. qRT-PCR analysis of Axin2 mRNA expression in MDA-MB-231 and BT20 cells following treatment with free FZD7 antibodies, FZD7-NS, PEG-NS, IgG-NS or no NS for 6 h. Cells were in the presence of 125 ng mL^{-1} Wnt3a for the final 4 h of treatment. By one-way ANOVA with posthoc Tukey (#) indicates $p < 0.05$ compared to cells treated with PEG-NS, free FZD7, and no NS, and (*) indicates $p < 0.05$ compared to cells treated with IgG-NS or no NS.

cell signaling, as they may be able to capitalize on multivalent binding effects for both signaling inhibition and additional therapies facilitated by the design of the nanocarrier. Ultimately, our results suggest that antibody-NP conjugates may be useful alternatives to freely delivered antibodies in both fundamental biological studies and treatment strategies that require efficient signal cascade interference.

2. Results and Discussion

2.1. Nanoshell Characterization

NS composed of silica cores ($\approx 120 \text{ nm}$) and thin gold shells ($\approx 15 \text{ nm}$) were synthesized according to previously published methods.^[40] Scanning electron microscopy (SEM) images indicated the NS had a highly monodisperse size distribution (Figure 2B). UV-vis spectrophotometry revealed the NS had a peak plasmon resonance at 830 nm (Figure 2C), which is important for their use as contrast agents for multiphoton microscopy to assess cellular binding, as described in detail later. Note that Figure 2C displays the extinction of NS from a single synthesis batch; the peak wavelength varied by several nanometers for each batch. For our studies, we developed three types of NS formulations: (1) NS coated with FZD7 antibodies and methoxy polyethylene glycol-thiol (mPEG-SH) (FZD7-NS), (2) NS coated with nonspecific IgG antibodies and mPEG-SH (IgG-NS), and (3) NS coated with only mPEG-SH (PEG-NS). Antibody and mPEG-SH attachment to NS was confirmed by dynamic light scattering (DLS), which showed increased hydrodynamic diameter and zeta potential upon functionalization compared to bare NS (Figure 2D). Further, the peak plasmon resonance shifted $\approx 20 \text{ nm}$ following NS functionalization with antibodies, indicating successful conjugation (Figure S1, Supporting Information). We conducted solution-based enzyme linked immunosorbent assays (ELISAs) to quantify antibody loading on NS, and NS with loading of at least 40 antibodies per NS were used for experiments.

2.2. Analysis of FZD7 Expression in TNBC Cells

We used MDA-MB-231 and BT20 TNBC cells, as well as MCF10A noncancerous breast cells, as models for our studies. Both MDA-MB-231 and BT20 cells are known to have overactive Wnt signaling mediated by FZD7 cell surface receptors.^[20] We validated the relative FZD7 expression of these cells versus MCF10A cells by immunohistochemical (IHC) staining and Western blotting (Figure 1C,D). Consistent with literature,^[20] we found that both MDA-MB-231 and BT20 cells express high levels of FZD7 relative to MCF10A cells, as indicated by the positive red stain in the IHC samples and by the amplified band density in Western blot samples.

2.3. Cell Selectivity and Binding Affinity of FZD7-NS and Free FZD7 Antibodies

We evaluated the ability of FZD7-NS and nontargeted NS to selectively bind TNBC cells using two-photon microscopy (TPM), in which NS act as natural contrast agents by emitting light in response to a pulsed near infrared laser tuned to the peak NS plasmon resonance wavelength.^[41] Following a 4 h incubation with FZD7-NS, PEG-NS, or no NS, TPM showed specific binding of FZD7-NS to TNBC cells but not to healthy cells, as indicated by the blue signal (Figure 3A). As expected, PEG-NS did not bind either cell type (Figure 3A).

To probe our hypothesis that FZD7-NS would bind TNBC cells with higher affinity than free FZD7 antibodies due to their multivalency, we employed a modified Langmuir isotherm model as described by Puig et al., which describes the binding of a free ligand, in this case FZD7-NS or free FZD7 antibodies, to an immobilized antigen, such as cells fixed to a plate.^[42] Using this model, we found an effective dissociation constant of $4.83 \times 10^{-10} \text{ M}$ for FZD7-NS, and $1.38 \times 10^{-8} \text{ M}$ for free FZD7 antibodies (Figure 3B). The lower effective dissociation constant for FZD7-NS compared to free FZD7 antibodies indicates that FZD7-NS have ≈ 100 -fold increased binding affinity to FZD7 cell surface receptors relative to freely delivered FZD7 antibodies. The data shown in Figure 3B is representative from three individual experiments for both FZD7-NS and free FZD7 antibodies. The averaged dissociation constant among all three experiments was $4.9 \times 10^{-10} \pm 1.73 \times 10^{-10} \text{ M}$ and $1.48 \times 10^{-8} \pm 1.48 \times 10^{-9} \text{ M}$ for FZD7-NS and free FZD7 antibodies, respectively. This study was critical since minimal research has investigated how increased binding affinity from antibody-nanoparticle conjugates correlates with oncogenic cell signaling blockade. Next, we investigated how this increased binding affinity correlates to Wnt signaling inhibition.

2.4. Wnt Signaling Inhibition Mediated by FZD7-NS

Since FZD7-NS could specifically bind TNBC cells with higher affinity than free FZD7 antibodies, we hypothesized that they could also manipulate Wnt signaling more effectively than free antibodies. To investigate this, we co-treated TNBC cells with either FZD7-NS, free FZD7 antibodies,

PEG-NS, IgG-NS, or no NS and the extracellular Wnt ligand Wnt3a. Overactive Wnt signaling is often due to extracellular Wnt proteins, particularly Wnt3a, that are available to bind overexpressed FZD7 receptors on TNBC cells.^[19,20] We determined the optimal concentration of Wnt3a to activate Wnt signaling by analyzing β -catenin expression in cells exposed to various concentrations of Wnt3a (Figure 4A) and found that β -catenin levels are maximized in MDA-MB-231 cells treated with at least 125 ng mL^{-1} Wnt3a. Since Wnt3a activates Wnt signaling through FZD7 receptors, we hypothesized that FZD7-NS would competitively bind FZD7 receptors in place of Wnt3a ligands to block Wnt stimulation and ultimately reduce β -catenin and Axin2 expression levels. Further, we expected FZD7-NS to be more effective at inhibiting Wnt signaling compared to free FZD7 antibodies, due to their enhanced binding affinity. As mentioned above, we treated MDA-MB-231 cells with FZD7-NS, PEG-NS, IgG-NS, free FZD7 antibodies, or no NS for 6 h and added 125 ng mL^{-1} Wnt3a for the final 4 h of the incubation to competitively bind FZD7 receptors. Importantly, free FZD7 antibodies were added to cells at $50 \mu\text{g mL}^{-1}$, which is ≈ 50 -fold more antibody than in cells treated with FZD7-NS. Western blotting revealed that cells treated with FZD7-NS had lower β -catenin protein levels than cells treated with free FZD7 antibodies (representative Western blot shown in Figure 4B). Comparing band densities from cells treated with IgG-NS relative to cells treated with PEG-NS revealed that both control NS types do not influence β -catenin levels to the same extent as FZD7-NS (Figure S2, Supporting Information).

The impact that FZD7-NS have on β -catenin levels was confirmed by immunofluorescence staining, which showed lower cytoplasmic and nuclear levels in cells treated with FZD7-NS compared to free antibody, PEG-NS, or no NS (Figure 4C). In this data, β -catenin was stained green with Alexa Fluor 488-conjugated secondary antibodies that bound to anti- β -catenin primary antibodies and nuclei were stained blue with 4',6-diamidino-2-phenylindole (DAPI). The images shown represent the average β -catenin nuclear fluorescence intensity in each treatment group from three individual experiments as quantified using ImageJ software (detailed analysis provided in the Experimental section). In these experiments, cells treated with free FZD7 antibodies were exposed to $50 \mu\text{g mL}^{-1}$ antibody, which is $\approx 50\times$ excess antibody compared to cells treated with FZD7-NS, demonstrating that multivalency plays a critical role in nanoparticle-mediated signal cascade interference. Interestingly, both immunofluorescence staining and Western blotting demonstrate that cells treated with PEG-NS may experience a modest effect on β -catenin levels compared to no NS. This indicates that NS alone may have an effect on Wnt signaling at the concentrations used in these experiments, although not to the same extent achieved when the NS are coated with FZD7 antibodies. This is not surprising given that NPs can inherently influence cell signaling processes.^[43,44] Regardless, the anti-FZD7 functionalization enables FZD7-NS to specifically bind TNBC cells overexpressing FZD7 receptors and results in greater knockdown of β -catenin than PEG-NS, ensuring that the effect is FZD7/Wnt-specific.

To confirm that FZD7-NS directly inhibit Wnt signaling specifically, we also investigated the effect of treating MDA-MB-231 and BT20 cells with FZD7-NS, IgG-NS, PEG-NS, or free FZD7 antibodies on the universal downstream Wnt target Axin2. The expression of Axin2 is often measured to assess activation or depletion of Wnt activity, as this avoids common experimental issues when studying β -catenin.^[45] Accordingly, Axin2 is considered the definitive marker of Wnt signaling activity. In TNBC cells, Axin2 expression is upregulated compared to healthy cells, particularly when activated by Wnt3a; in our studies, treatment with 125 ng mL^{-1} Wnt3a resulted in an 8.2-fold increase in Axin2 expression (Figure S3, Supporting Information).^[45] We found that both TNBC cell lines that were co-treated with FZD7-NS and Wnt3a experienced a $\approx 60\%$ decrease in Axin2 mRNA expression compared to untreated cells, indicating significant downstream Wnt inhibition (Figure 5,* and # indicate $p < 0.05$ by ANOVA with posthoc Tukey, $n = 3$). Cells treated with free FZD7 antibodies (at $\approx 50\times$ excess antibodies), IgG-NS, or PEG-NS experienced minimal effects on Axin2 mRNA expression relative to untreated cells.

Lastly, we investigated how inhibited Wnt signaling influences cell viability by treating MDA-MB-231 cells with FZD7-NS, IgG-NS, PEG-NS, or no NS and Wnt3a. We assessed cell viability using an Alamar blue assay, which measures the cells' metabolic activity. Since Wnt signaling is critical for TNBC cell proliferation and disease progression, we anticipated that FZD7-NS would decrease cell viability by blocking Wnt signaling activation. After a 16 h incubation with each treatment group, we found that FZD7-NS decreased cell viability $\approx 25\%$ relative to controls (Figure 6), which is substantial given that 16 h is less than one doubling time for the cell lines evaluated. We did not see significant decreases in cell viability in any control groups, including cells treated with an excess of free FZD7 antibodies, which indicates that nanoparticle multivalency is playing a critical role for Wnt signaling inhibition and cell growth.

In summary, we developed and evaluated FZD7-NS to demonstrate that antibodies conjugated to the surface of

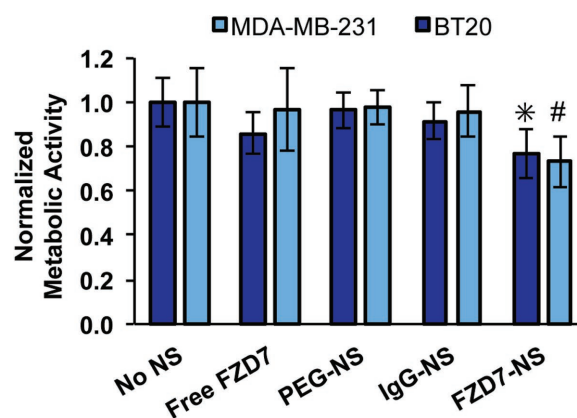


Figure 6. Cell viability analysis 16 h post-treatment with FZD-NS, IgG-NS, PEG-NS, free FZD7 antibodies, or no NS. (#) $p < 0.05$ compared to cells treated with IgG-NS, PEG-NS, free FZD7 antibodies, or no NS. (*) $p < 0.05$ compared to cells treated with IgG-NS, PEG-NS, and no NS by one way ANOVA with post hoc Tukey.

NS can exploit the multivalent binding effects afforded by nanocarriers relative to free antibodies in order to potently manipulate downstream gene expression. The ability to inhibit oncogenic signaling cascades, such as Wnt signaling, with ligand-targeted NPs is an underexplored area in the field of nanomedicine. Our data indicate that using targeted NPs to block native ligands from binding their intended receptors has substantial promise as a therapeutic strategy. Further, we show that using nanocarriers as delivery agents leads to enhanced signaling impacts with lower doses compared to free antibody delivery. These findings support further development of NPs functionalized with ligands that elicit known cell signaling responses to improve upon their therapeutic capabilities. The success of many antibody therapies used clinically to treat cancer is limited by high required dosages, which make treatment expensive and may lead to adverse side effects. As demonstrated here, antibodies conjugated to nanoparticles may lead to lower required dosages and therefore fewer side effects than freely delivered antibodies. Ultimately, this approach may be applied to a wide range of NP cores functionalized with various antagonistic antibodies to enhance disease management.

3. Conclusions

NS coated with FZD7 antibodies and mPEG-SH to study the effects of nanoparticle multivalency on signal cascade interference to antagonize the Wnt signaling pathway is demonstrated. We show that FZD7-NS bind TNBC cells sufficiently to reduce β -catenin and Axin2 expression, as evidenced by immunofluorescence staining, Western blotting, and qRT-PCR. More specifically, cells treated with FZD7-NS in the presence of 125 ng mL⁻¹ Wnt3a experienced \approx 60% decrease in Axin2 expression relative to untreated cells, indicating significant inhibition of the Wnt signaling pathway. This inhibited Wnt signaling resulted in \approx 25% decrease in cell viability only 16 h post treatment with FZD7-NS. Excitingly, the Wnt inhibitory effects of FZD7-NS were much greater than those observed when cells were treated with 50-fold more free FZD7 antibodies. We attribute the enhanced Wnt inhibitory effects of FZD7-NS relative to free FZD7 antibodies to their multivalency, as we found that FZD7-NS bind TNBC cells with effective binding affinities two orders of magnitude higher than free FZD7 antibodies. Together, these results indicate that binding affinity correlates to enhanced signaling inhibition and therapeutic effects, and that antibody-NP conjugates may overcome the dose limitations of free antibody therapeutics. Future in vivo studies will need to be performed to validate the therapeutic implications of multivalent binding in a complex biological system, and additional studies that investigate the role of nanoparticle size in the ability to suppress oncogenic signaling with antibody-NP conjugates would provide important insight to structure/function relationships of these nanomaterials. As our studies demonstrate that antibody-NP conjugates offer substantial benefits over freely delivered antibodies, this work supports further development of functionalized NPs to actively target diseased cells and to control aberrant signaling pathways implicated in disease progression.

4. Experimental Section

Nanoshell Synthesis and Antibody Functionalization: Nanoshells with 120 nm diameter spherical silica cores and \approx 15 nm thick gold shells were synthesized by the method of Oldenburg et al. as previously described.^[40] Briefly, colloidal gold (\approx 2–3 nm) prepared according to Duff et al.^[46] was combined with silica cores coated with 3-aminopropyltriethoxysilane (Nanocomposix) and reacted for 3 d at room temperature. Unbound colloidal gold was removed by centrifugation (2800 rpm, 25 min) and additional gold was reduced with formaldehyde onto the gold nucleation sites on the silica cores to form complete gold shells.

To conjugate either rabbit anti-human FZD7 (Pierce) or mouse anti-human IgG (Rockland) antibodies to NS, anti-FZD7 or anti-IgG were linked to 2 kDa orthopyridyl disulfide-polyethylene glycol-succinimidyl valerate (OPSS-PEG-SVA, Laysan Bio) in sodium bicarbonate. Nine parts OPSS-PEG-SVA were reacted with 1 part antibody at a 2:1 PEG-to-antibody molar ratio overnight at 4 °C to form OPSS-PEG-FZD7 or OPSS-PEG-IgG. Then, the PEGylated antibodies were purified by dialysis using microdialysis devices with a 10 kDa molecular weight cutoff (Spectrum Labs). Antibodies were purified against 1 \times phosphate buffered saline (PBS) at 4 °C, and the dialysis buffer was changed three times before collecting the antibodies from the devices. Finally, OPSS-PEG-FZD7 or OPSS-PEG-IgG was added to NS suspended in purified water at 1250 molecules per NS and reacted for 4 h at 4 °C. To enhance NS stability and eliminate nonspecific protein adsorption, 5 kDa methoxy polyethylene glycol-thiol (mPEG-SH, Laysan Bio) was added to the NS solutions to a final concentration of 2.5×10^{-6} M and reacted overnight at 4 °C. Control NS were coated only with 5 kDa mPEG-SH. Lastly, NS were purified via centrifugation (1500 g, 10 min) to remove unbound molecules with the supernatant. Purified PEG-NS, FZD7-NS, or IgG-NS were stored at 4 °C in purified water until use.

Nanoshell Characterization: Bare NS, PEG-NS, IgG-NS, and FZD7-NS were characterized by UV-vis spectrophotometry (Cary60, Agilent), scanning electron microscopy (Hitachi S4700), and DLS and/or zeta potential measurements (ZetaSizer NanoZS, Malvern). For UV-vis spectrophotometry, the authors first determined the baseline by scanning water in a disposable cuvette. Then, NS were diluted in water in disposable cuvettes, read on the spectrophotometer (from 1100 to 400 nm, 2400 nm min⁻¹ scan speed), and NS concentration was determined using the peak absorbance as determined by spectrophotometry and Beer's law. Similar sample preparations were completed for dynamic light scattering and zeta potential measurements. NS samples for SEM were prepared by first diluting NS in ethanol and then drying samples directly onto SEM sample holders prior to imaging. Conjugation of anti-FZD7 or anti-IgG to NS was confirmed by a solution-based ELISA as the authors previously described.^[35] Briefly, FZD7-NS, IgG-NS, or PEG-NS were incubated with 10 μ g mL⁻¹ horseradish peroxidase (HRP)-conjugated anti-rabbit IgG (HRP-AR, KPL) for 1 h at room temperature. Samples were pelleted by centrifugation (500 g, 5 min, thrice) to remove unbound secondary antibodies in the supernatant and then suspended in 3% bovine serum albumin in PBS (PBSA). Samples were developed in 3,3',5,5'-tetramethylbenzidine (TMB, Sigma-Aldrich) for 15 min and then sulfuric acid was added to stop the reaction. Absorbance at 450 nm was measured on a Cary60 spectrophotometer and compared to a standard curve of known HRP concentration to calculate the number of FZD7 or IgG antibodies per NS.

Cell Culture: MDA-MB-231 and BT20 TNBC cells were purchased from American Type Culture Collection (ATCC) and cultured in Dulbecco's Modified Eagle Medium (DMEM) or Eagle's Minimum Essential Medium (EMEM), respectively, each supplemented with 10% fetal bovine serum (FBS) and 1% penicillin–streptomycin (Life Technologies). Noncancerous MCF-10A breast epithelial cells were kindly provided by Dr. Kenneth Van Golen and were cultured in a 50:50 DMEM and F12 base medium supplemented with 5% FBS, 10 $\mu\text{g mL}^{-1}$ insulin, 0.5 $\mu\text{g mL}^{-1}$ hydrocortisone, 50 $\mu\text{g mL}^{-1}$ bovine pituitary extract, 20 ng mL^{-1} epidermal growth factor, and 100 ng mL^{-1} cholera toxin. Cells were cultured in T25 or T75 cell culture flasks and incubated at 37 °C in a 5% CO_2 environment.

Immunohistochemical Staining of FZD7: MDA-MB-231, BT20, and MCF-10A cells were detached from cell culture flasks with trypsin-ethylenediaminetetraacetic acid (EDTA), plated in 24-well plates at 40 000 cells per well, and incubated overnight. Then, cells were fixed with 4% formaldehyde and rinsed 3 \times with PBS. Endogenous peroxidases were blocked with 3% hydrogen peroxide for 10 min and nonspecific protein interactions were blocked with 3% PBSA for 60 min. Mouse anti-human FZD7 antibodies (LifeSpan Biosciences) diluted in PBSA to 5 $\mu\text{g mL}^{-1}$ were added to each well and samples incubated overnight at 4 °C. Anti-FZD7 antibodies were removed, samples were rinsed 3 \times in PBS, and then HRP-anti-mouse IgG (Sigma-Aldrich) diluted to 3 $\mu\text{g mL}^{-1}$ was added for 60 min at room temperature. Samples were rinsed 3 \times in PBS and 3-amino-9-ethylcarbazole (Sigma-Aldrich) was added for 20 min to stain bound HRP secondary antibodies. To stop the reaction, samples were rinsed with PBS. Stained cells were imaged on a Zeiss Axioobserver Z1 inverted fluorescence microscope using bright-field light capabilities and a color camera. This same microscope was used to image samples for all experiments except where indicated. IHC experiments were conducted at least three times, and a minimum of three images were acquired per treatment group in each experiment.

Specific Binding of FZD7-NS to TNBC Cells: MDA-MB-231 and MCF-10A cells were detached from culture flasks with trypsin-EDTA, seeded at 100 000 cells per well in 8-well chambered coverglass and incubated overnight. Cells were treated with FZD7-NS or PEG-NS at 8.2×10^9 NS mL^{-1} (corresponding to an optical density (OD) of 3 at 800 nm), or with no NS, in complete media for 4 h at 37 °C and then rinsed 3 \times with PBS to remove unbound NS. Cells were then fixed with 4% formaldehyde and imaged with a Zeiss LSM 510 NLO multiphoton microscope equipped with a pulsed Ti:sapphire laser. The laser was tuned to the peak resonance wavelength of the NS (which was ≈ 830 nm but varied by experiment since different NS batches have different resonance wavelengths), and cells were imaged with a 20 \times objective in combination with a long pass dichroic mirror. This experiment was repeated at least three times for each combination of cell type and nanoparticle type, and the sample wells were imaged in at least three locations.

Binding Affinity of FZD7-NS and Free FZD7: MDA-MB-231 cells were seeded at 15 000 cells per well in 96 well plates. Following overnight incubation, cells were fixed with 4% formaldehyde and rinsed with 1 \times PBS. Cells were treated with 3% hydrogen peroxide for 10 min, followed by 3% PBSA for 2 h. FZD7-NS ($0-7.36 \times 10^{-9} \times \text{M}$ antibody) or free FZD7 solutions ($0-133.3 \times 10^{-9} \times \text{M}$) were prepared in ultrapure water and were added to cells and incubated at room temperature for 1.5 h. Samples were then washed 3 \times with 1% PBSA with 0.01% Tween-20 (PBST) for 10 min each, and 2.5 $\mu\text{g mL}^{-1}$ HRP-anti-rabbit secondary antibodies (400 \times dilution)

were added for 1 h. After washing 3 \times with PBST for 15 min each, samples were developed in 3,3',5,5'-TMB (Sigma-Aldrich) and then sulfuric acid was added to stop the reaction. Absorbance at 450 nm was measured on a Cary60 spectrophotometer and plotted versus FZD7 antibody concentration. Data was fit to a modified Langmuir isotherm model as described by Puig et al.^[42] to find the effective dissociation constant using the equation $\text{OD} = \frac{\text{Ab}_{\text{conc}}}{K_{\text{D}}^{\text{eff}} + \text{Ab}_{\text{conc}}}$. In this equation, Ab_{conc} is the concentration of antibody added to cells and $K_{\text{D}}^{\text{eff}}$ is the effective dissociation constant. Further, OD is optical density at each antibody concentration normalized according to the equation $\text{OD} = \frac{\text{OD}_{\text{raw}} - \text{OD}_{\text{back}}}{\text{OD}_{\text{high}} - \text{OD}_{\text{back}}}$, where OD_{raw} is the initial optical density reading prior to any calculations, OD_{back} is the optical density of background signal (cells treated with no primary antibody and treated with secondary antibody), and OD_{high} is the optical density of the highest (saturated) signal. Binding affinity experiments were conducted with at least two replicates per antibody concentration, and the experiments were conducted three times.

Immunofluorescence Staining for β -Catenin Expression: MDA-MB-231 cells were seeded at 30 000 cells per well in 8-well chambered coverglass, incubated overnight, and serum starved for 24 h. Then, cells were treated with FZD7-NS or PEG-NS at a density of 2.7×10^{10} NS mL^{-1} , or 50 $\mu\text{g mL}^{-1}$ free FZD7 antibodies for 6 h in serum free media. Wnt3a (125 ng mL^{-1}) was added for the final 4 h of the treatment period. Control samples received no NS. Cells were rinsed 3 \times with PBS to remove unbound nanoparticles, fixed with 4% formaldehyde, and permeabilized with 0.5% Triton-X in PBSA for 10 min. Next, samples were blocked with 10% PBSA for 30 min. Mouse anti-human β -catenin antibody (Santa Cruz) diluted to 2 $\mu\text{g mL}^{-1}$ in PBST was incubated with cells overnight at 4 °C. Samples were washed 3 \times with PBSA and incubated with AlexaFluor 488-conjugated goat anti-mouse IgG (ThermoFisher Scientific) diluted to 2 $\mu\text{g mL}^{-1}$ in PBST for 1 h at room temperature. Slides were mounted with Vectashield Antifade Mounting Medium with DAPI (VWR) and imaged under fluorescence microscopy on a Zeiss Axioobserver Z1 microscope with the EGFP (ex. 488 nm, em. 509 nm) and DAPI filter sets. β -catenin nuclear signal intensity was quantified in ImageJ software. First, the nuclear and β -catenin channels were split. A threshold was applied to the nuclear channel to define individual nuclei as regions of interest (ROIs). Then, the average nuclear intensity was analyzed in the β -catenin channel using the ROIs defined by the nuclear threshold. The images shown represent the mean fluorescence intensity across three replicates for each treatment group with three or five images acquired in each well. Although the exact number of cells in each field of view varied, the authors imaged at least 400 cells per treatment group in each experiment.

Western Blot Analysis for β -Catenin or Frizzled7 Expression: Cells were lysed in RIPA buffer (Amersco) supplemented with Halt Protease Inhibitory Cocktail (Life Technologies) per the manufacturer's instructions. Lysate from untreated MDA-MB-231, BT20, and MCF-10A cells was used to assess baseline Frizzled7 expression. To assess β -catenin expression, MDA-MB-231 or BT20 cells were seeded at 50 000 cells per well in 24 well plates, incubated overnight, and serum starved for 24 h. Cells were treated in an identical manner as described for immunofluorescence staining experiments, and at least three experimental replicates were completed. Following the 6 h incubation, cells were washed 1 \times with PBS and lysed in RIPA buffer (Amersco) supplemented with Halt Protease Inhibitor Cocktail

(Life Technologies) per the manufacturer's instructions. Protein concentration was determined using a DC Protein Assay (BioRad). 10 µg of protein was separated on 8% Bis–tris gels at 165 V for 35 min. Then, the protein was transferred to nitrocellulose membranes for 12.5 min using the Pierce Power System (Thermo Scientific). Membranes were blocked for 90 min in tris buffered saline with 0.1% Tween-20 (TBST) and 5% BSA and then incubated with mouse anti-human β-catenin antibodies (Santa Cruz) diluted to 0.4 µg mL⁻¹ (1:500) or mouse anti-human Frizzled7 antibodies (Santa Cruz) diluted to 0.5 µg mL⁻¹, in TBST with 5% BSA overnight at 4 °C. Mouse anti-human β-actin diluted to 0.2 µg mL⁻¹ (1:5000) was used as the normalization control. After overnight incubation, membranes were washed 3× in TBST and incubated with HRP-anti-mouse IgG (Santa Cruz) diluted to 0.02 µg mL⁻¹ (1:5000) in TBST with 5% BSA for 1 h at room temperature. Membranes were washed 3× in TBST, followed by 1× in TBS (without Tween-20) and protein bands were visualized using an Amersham enhanced chemiluminescence detection solution (GE Healthcare). For the Frizzled7 Western blot, membranes were incubated with stripping buffer (Amresco) for 30 min and rinsed 3× with TBST prior to incubation with the β-actin antibodies. In these experiments, the band densities were quantified in ImageJ, and the blot shown represents the average band density across experiments.

qRT–PCR Analysis for Axin2 mRNA Expression: MDA-MB-231 or BT20 cells were treated with free FZD7 antibodies, FZD7-NS, PEG-NS, IgG-NS, or no NS in an identical manner to immunofluorescence experiments. Following the 6 h incubation, total RNA was extracted using the Isolate II RNA Mini Kit (Bioline) per manufacturer instructions. PCR reactions were performed using the SensiFAST SYBR No-ROX One-Step Kit (Bioline). Reactions pre-incubated for 20 min at 48 °C and then for 10 min at 95 °C followed by 40 cycles of 95 °C for 10 s, 60 °C for 20 s, and 72 °C for 20 s (Roche LightCycler 96). The primer sequences (Life Technologies) used for qRT-PCR were: (1) GAPDH Forward: ACAGTCAGCCGATCTTCTT, (2) GAPDH Reverse: ACGACCAAATCCGTTGACTC, (3) Axin2 Forward: TTATGCTTTGCACTACGTCCTCCA, (4) Axin2 Reverse: CGCAACATGTCAACCTCAGAC. The Delta-Delta Ct method was used to calculate relative Axin2 mRNA expression, and the data shown are the means ± standard deviations of triplicate experiments. Data was analyzed by ANOVA with posthoc Tukey.

Analysis of Cellular Metabolic Activity: MDA-MB-231 or BT20 cells were treated with free FZD7 antibodies, FZD7-NS, PEG-NS, IgG-NS, or no NS in an identical manner to immunofluorescence experiments. After 16 h incubation, the NS and Wnt3a-containing media was replaced with AlamarBlue reagent (Thermo Fisher) per manufacturer instructions. After 4 h, the samples' fluorescence was read on a Hybrid Synergy H1M plate reader, and data was normalized to untreated controls for each cell line. The data shown are the means ± standard deviations of three individual experiments, each with three wells that were treated as biological replicates. The data was analyzed by one-way ANOVA with posthoc Tukey–Kramer.

Supporting Information

Supporting Information is available from the Wiley Online Library or from the author.

Acknowledgements

The authors thank Deborah Powell and Jean Ross for assistance with scanning electron microscopy, Michael Moore for assistance with two-photon microscopy, and Dr. Joshua Morgan for assistance with molecular biology techniques. This work was supported with funding from the University of Delaware Research Foundation, by Grant #IRG-14-251-07-IRG from the American Cancer Society, and by a Maximizing Investigator's Research Award (MIRA) from the National Institute of General Medical Sciences (NIGMS) of the National Institutes of Health (NIH) under grant number R35GM119659. Additionally, the Delaware INBRE program supported this project, with a grant from NIH NIGMS (P20-GM103446). The content is solely the responsibility of the authors and does not necessarily represent the views of the NIH or the American Cancer Society.

Conflict of Interest

The authors declare no conflict of interest.

- [1] M. X. Sliwkowski, I. Mellman, *Science* **2013**, *341*, 1192.
- [2] A. M. Scott, J. P. Allison, J. D. Wolchok, *Cancer Immun.* **2012**, *12*, 1.
- [3] A. M. Scott, J. D. Wolchok, L. J. Old, *Nat. Rev. Cancer* **2012**, *12*, 278.
- [4] H. Samaranyake, T. Wirth, D. Schenkwein, J. K. Raty, S. Yla-Herttuala, *Ann. Med.* **2009**, *41*, 322.
- [5] M. Neyt, *Am. J. Cancer* **2006**, *5*, 19.
- [6] T. M. Allen, *Nat. Rev. Cancer* **2002**, *2*, 750.
- [7] R. Weissleder, K. Kelly, E. Y. Sun, T. Shtatland, L. Josephson, *Nat. Biotechnol.* **2005**, *23*, 1418.
- [8] Y. A. Mahamodhossen, W. Liu, Z. Rong-Rong, *Med. Oncol.* **2013**, *30*, 653.
- [9] C. L. Griffiths, J. L. Olin, *J. Pharm. Pract.* **2012**, *25*, 319.
- [10] H. Clevers, R. Nusse, *Cell* **2012**, *149*, 1192.
- [11] T. D. King, M. J. Suto, Y. Li, J. *Cell. Biochem.* **2012**, *113*, 13.
- [12] S. Angers, R. T. Moon, *Nat. Rev. Mol. Cell Biol.* **2009**, *10*, 468.
- [13] J. N. Anastas, R. T. Moon, *Nat. Rev. Cancer* **2013**, *13*, 11.
- [14] T. Reya, H. Clevers, *Nature* **2005**, *434*, 843.
- [15] B. Lustig, B. Jerchow, M. Sachs, S. Weiler, T. Pietsch, U. Karsten, M. van De Wetering, H. Clevers, P. M. Schlag, W. Birchmeier, J. Behrens, *Mol. Cell. Biol.* **2002**, *22*, 1184.
- [16] E. Jho, T. Zhang, C. Domon, C.-K. Joo, J.-N. Freund, F. Costantini, *Mol. Cell. Biol.* **2002**, *22*, 1172.
- [17] Z.-Q. Wu, T. Brabletz, E. Fearon, A. L. Willis, C. Y. Hu, X.-Y. Li, S. J. Weiss, *Proc. Natl. Acad. Sci. USA* **2012**, *109*, 11312.
- [18] S. Segditsas, I. Tomlinson, *Oncogene* **2006**, *25*, 7531.
- [19] T. D. King, W. Zhang, M. J. Suto, Y. Li, *Cell. Signaling* **2012**, *24*, 846.
- [20] L. Yang, X. Wu, Y. Wang, K. Zhang, J. Wu, Y.-C. Yuan, X. Deng, L. Chen, C. C. H. Kim, S. Lau, G. Somlo, Y. Yen, *Oncogene* **2011**, *30*, 4437.
- [21] N. Pode-Shakked, O. Harari-Steinberg, Y. Haberman-Ziv, E. Rom-Gross, S. Bahar, D. Omer, S. Metsuyanin, E. Buzhor, J. Jacob-Hirsch, R. Goldstein, M. Mark-Danieli, B. Dekel, *Oncogene* **2011**, *30*, 1664.
- [22] A. Gurney, F. Axelrod, C. J. Bond, J. Cain, C. Chartier, L. Donigan, M. Fischer, A. Chaudhari, M. Ji, A. M. Kapoun, A. Lam, S. Lazetic, S. Ma, S. Mitra, I.-K. Park, K. Pickell, A. Sato, S. Satyal, M. Stroud, H. Tran, W.-C. Yen, J. Lewicki, T. Hoey, *Proc. Natl. Acad. Sci. USA* **2012**, *109*, 11717.

- [23] OncoMed Pharmaceuticals, Inc. *ClinicalTrials.gov [Internet]*, National Library of Medicine, Bethesda, MD **2013**, <https://clinicaltrials.gov/ct2/show/NCT02005315>, NLM identifier: NCT02005315 (cited March 2017).
- [24] L. B. Carpin, L. R. Bickford, G. Agollah, T.-K. Yu, R. Schiff, Y. Li, R. A. Drezek, *Breast Cancer Res. Treat.* **2011**, *125*, 27.
- [25] A. R. Lowery, A. M. Gobin, E. S. Day, N. J. Halas, J. L. West, *Int. J. Nanomed.* **2006**, *1*, 149.
- [26] P. Guo, J. You, J. Yang, D. Jia, M. A. Moses, D. T. Auguste, *Mol. Pharm.* **2014**, *11*, 755.
- [27] H. Lee, D. Dam, J. Ha, J. Yue, T. Odom, *ACS Nano* **2015**, *9*, 9859.
- [28] W. Jiang, B. Y. S. Kim, J. T. Rutka, W. C. W. Chan, *Nat. Nanotechnol.* **2008**, *3*, 145.
- [29] S. K. Kim, L. Huang, *J. Controlled Release* **2012**, *157*, 279.
- [30] S. A. Jensen, E. S. Day, C. H. Ko, L. a Hurley, J. P. Luciano, F. M. Kouri, T. J. Merkel, A. J. Luthi, P. C. Patel, J. I. Cutler, W. L. Daniel, A. W. Scott, M. W. Rotz, T. J. Meade, D. a Giljohann, C. a Mirkin, A. H. Stegh, *Sci. Transl. Med.* **2013**, *5*, 209ra152.
- [31] F. M. Kouri, L. A. Hurley, W. L. Daniel, E. S. Day, Y. Hua, L. Hao, C. Y. Peng, T. J. Merkel, M. A. Queisser, C. Ritner, H. Zhang, C. David James, J. I. Sznajder, L. Chin, D. A. Giljohann, J. A. Kessler, M. E. Peter, C. A. Mirkin, A. H. Stegh, *Genes Dev.* **2015**, *29*, 732.
- [32] I. Ahmad, T. M. Allen, *Cancer Res.* **1992**, *52*, 4817.
- [33] J. W. Park, K. Hong, D. B. Kirpotin, G. Colbern, R. Shalaby, J. Baselga, Y. Shao, U. B. Nielsen, J. D. Marks, D. Moore, D. Papahadjopoulos, C. C. Benz, *Clin. Cancer Res.* **2002**, *8*, 1172.
- [34] E. C. Dreaden, S. C. Mwakwari, Q. H. Sodji, A. K. Oyelere, M. A. El-sayed, *Bioconjugate Chem.* **2009**, *20*, 2247.
- [35] E. S. Day, L. Zhang, P. A. Thompson, J. A. Zawaski, C. C. Kaffes, M. W. Gaber, S. M. Blaney, J. L. West, *Nanomedicine* **2012**, *7*, 1133.
- [36] J. M. Stern, V. V. K. Solomonov, E. Sazykina, J. A. Schwartz, S. C. Gad, G. P. Goodrich, *Int. J. Toxicol.* **2015**, *35*, 38.
- [37] C. Loo, A. Lin, L. Hirsch, M.-H. Lee, J. Barton, N. Halas, J. West, R. Drezek, *Technol. Cancer Res. Treat.* **2004**, *3*, 33.
- [38] C. Loo, L. Hirsch, M.-H. Lee, E. Chang, J. West, N. Halas, R. Drezek, *Opt. Lett.* **2005**, *30*, 1012.
- [39] M. L. Li, J. C. Wang, J. a Schwartz, K. L. Gill-Sharp, G. Stoica, L. V Wang, *J. Biomed. Opt.* **2009**, *14*, 010507.
- [40] S. J. Oldenburg, R. D. Averitt, S. L. Westcott, N. J. Halas, *Chem. Phys. Lett.* **1998**, *288*, 243.
- [41] L. Bickford, J. Sun, K. Fu, N. Lewinski, V. Nammalvar, J. Chang, R. Drezek, *Nanotechnology* **2008**, *19*, 315102.
- [42] H. De Puig, I. Bosch, M. Carre, K. Hamad-schi, *Bioconjugate Chem.* **2017**, *28*, 230.
- [43] J. Rauch, W. Kolch, S. Laurent, M. Mahmoudi, *Chem. Rev.* **2013**, *113*, 3391.
- [44] F. Marano, S. Hussain, F. Rodrigues-Lima, A. Baeza-Squiban, S. Boland, *Arch. Toxicol.* **2011**, *85*, 733.
- [45] S. Maubant, B. Tesson, V. Maire, M. Ye, G. Rigai, D. Gentien, F. Cruzalegui, G. C. Tucker, S. Roman-Roman, T. Dubois, *PLoS One* **2015**, *10*, 1.
- [46] D. G. Duff, A. Baiker, P. P. Edwards, *Langmuir* **1993**, *272*, 2301.

Received: February 17, 2017
Revised: March 26, 2017
Published online: